Supplementary materials: Observation of Two-Dimensional Acoustic Bound States in the Continuum

Marc Martí-Sabaté,[1,2] Junfei Li,[3] Bahram Djafari-Rouhani,[4] Steven A. Cummer,[5] and Dani Torrent[1,*]

[1] *GROC, UJI, Institut de Noves Tecnologies de la Imatge (INIT), Universitat Jaume I, 12071, Castelló de la Plana, Spain*
[2] *Department of Mathematics, Imperial College London, London SW7 2AZ, United Kingdom*
[3] *School of Mechanical Engineering, Purdue University, West Lafayette, Indiana 47907, USA*
[4] *IEMN, University of Lille, Cité scientifique, 59650 Villeneuve d'Ascq, France*
[5] *Department of Electrical and Computer Engineering, Duke University, Durham, North Carolina 27708, USA*

SUPPLEMENTARY NOTE 1: BIC DESIGN THEORY: UNCOVERED PLATE

Let's assume that we have an infinitely periodic waveguide with a bunch of holes on it. The acoustic field at any position of the unit cell of the waveguide is

$$P(\boldsymbol{r}) = \sum_{\boldsymbol{G}} (B_G e^{iq_G z} + A_G e^{-iq_G z}) e^{i\boldsymbol{k_G}\cdot\boldsymbol{r}}, \tag{S1}$$

where G are the modes of the reciprocal lattice, $q_G = \sqrt{\omega^2/c^2 - |\mathbf{k_G}|^2}$. No incident field will be considered, that is to say, $A_G = 0$, as we are interested in the proper modes of the system. Then, the acoustic pressure field and the normal velocity field can be written

$$P(\boldsymbol{r}) = \sum_{G} B_G e^{iq_G z} e^{i\boldsymbol{k_G}\boldsymbol{r}} \tag{S2}$$

$$v_n(\boldsymbol{r}) = \sum_{G} \frac{iq_G}{k_b z_b} B_G e^{iq_G z} e^{i\boldsymbol{k_G}\boldsymbol{r}}, \tag{S3}$$

being z_b the acoustic impedance of the medium. Concerning the acoustic field inside the holes, only the main resonance of each hole will be considered, and the boundaries with the solid material are considered rigid. Therefore, the pressure field and the normal velocity field inside the hole are

$$P_\alpha(\boldsymbol{r}) = e^{i\boldsymbol{k}\mathbf{R}_\alpha} B_\alpha \frac{\cos\left(k_b(z + L_\alpha)\right)}{\sin\left(k_b L_\alpha\right)} \tag{S4}$$

$$v_{n\alpha}(\boldsymbol{r}) = \frac{-e^{i\boldsymbol{k}\mathbf{R}_\alpha}}{z_b} B_\alpha \frac{\sin\left(k_b(z + L_\alpha)\right)}{\sin\left(k_b L_\alpha\right)}. \tag{S5}$$

Next, mode matching at $z = 0$ plane is applied in order to match modes from the waveguide and modes from the boreholes (resonant cavities). Applying continuity to the integral of the pressure field in the area of a hole and continuity of the velocity field in the unit cell [1], two equations are obtained:

$$\sum_{G} B_G e^{i\boldsymbol{G}\mathbf{R}_\alpha} H_{\alpha G} = B_\alpha \cot\left(k_b L_\alpha\right) \tag{S6}$$

and

$$-\frac{iq_G}{k_b} B_G = \sum_{\beta} f_\beta e^{-i\boldsymbol{G}\mathbf{R}_\beta} H_{\beta G} B_\beta, \tag{S7}$$

where $H_{\alpha G} = \frac{1}{\Omega_\alpha}\int_{\Omega_\alpha} e^{i\boldsymbol{k_G}(\boldsymbol{r}-\mathbf{R}_\alpha)}d\Omega_\alpha$ and $f_\alpha = \frac{\Omega_\alpha}{\Omega_C}$ is the cavity's filling fraction, with Ω_c and Ω_α being the areas of the unit cell and the cavity α. After substituting B_G coefficients from equation (S7) into equation (S6), we get a system of equations such that:

$$\sum_\beta [\delta_{\alpha\beta}\cot(k_b L_\alpha) - i\chi_{\alpha\beta}]B_\beta = 0, \tag{S8}$$

where $\chi_{\alpha\beta}$ is

$$\chi_{\alpha\beta} = \sum_{\boldsymbol{G}} \frac{k_b}{q_G}\cot(q_G L_\alpha) f_\beta e^{i\boldsymbol{G}\mathbf{R}_{\alpha\beta}} H_{\alpha G} H_{\beta H}. \tag{S9}$$

$H_{\alpha G}$ can be simplified by assuming that all the holes in the system have the same depth L_α and the same radius R_a. Thus, $H_{\alpha G}$ is no longer dependent on the resonator, as every resonator has the same geometric and physical properties. Due to its circular section,

$$H_G = \frac{2}{R_a|\boldsymbol{k_G}|} J_1(R_a|\boldsymbol{k_G}|). \tag{S10}$$

Therefore,

$$\chi_{\alpha\beta} = \sum_G \frac{4\pi k_b}{|\boldsymbol{k_G}|^2 q_G \Omega_c} J_1^2(|\boldsymbol{k_G}|R_a) e^{i\boldsymbol{G}\mathbf{R}_{\alpha\beta}}. \tag{S11}$$

In the following, we want to have only one circle of resonators in our system. Thus, the limits of the unit cell will tend to infinity, such that

$$\lim_{a\to\infty} \frac{1}{\Omega_c}\sum_{\boldsymbol{G}} f(\boldsymbol{k}+\boldsymbol{G}) = \frac{1}{(2\pi)^2}\int\int f(\boldsymbol{k})d\boldsymbol{k} \tag{S12}$$

The sum over the reciprocal modes $\mathbf{G}$ is now an integral over $\mathbf{k}$. After changing to cylindrical coordinates and applying addition therem, the following expression is obtained for $\chi_{\alpha\beta}$

$$\chi_{\alpha\beta} = 2\sum_{n=-\infty}^{+\infty} (-1)^n e^{-2\pi i\beta n/N} e^{2\pi i\alpha n/N} I_{uncov}(n), \tag{S13}$$

where

$$I_{uncov}(n) = \int_0^{+\infty} \frac{k_b}{q_k k} J_1^2(kR_a) J_n^2(kR_0) dk. \tag{S14}$$

The integral term $I_{uncov}(n)$ has both real and imaginary part. Due to the symmetry of both the cluster and the operator, the following relation between scattering coefficients B_α can be applied [2, 3]:

$$B_\alpha = e^{2\pi i\ell\alpha/N} B_0, \tag{S15}$$

with ℓ being the resonant index. The system of equations in equation S8 gets reduced to a single equation, decoupled in two different conditions

$$\cot(k_b L_\alpha) = 2N(-1)^\ell \int_{k_b}^{\infty} \frac{k_b}{k|q_k|} J_1^2(kR_a) J_\ell^2(kR_0) dk \tag{S16}$$

$$0 = \int_0^{k_b} \frac{k_b}{k|q_k|} J_1^2(kR_a) J_\ell^2(kR_0) dk. \tag{S17}$$

Equation (S17) can not be satisfied, avoiding the possibility of having a real BIC for the uncovered plate. Nevertheless, at low frequency, the behaviour of the function inside the integral is governed by the term $J_\ell^2(kR_0)$. Function $J_1^2(kR_\alpha)$ has stronger effect in the high frequency regime. A mode with good quality factor can be designed by properly matching the frequency and the radius of the cluster to coincide with one of the zeros of $J_\ell^2(kR_0)$. Then, evaluating the integral term in equation (S16), a value for the depth of the holes can be obtained.

SUPPLEMENTARY NOTE 2: BIC DESIGN THEORY: COVERED PLATE

Starting from equation (S1), the wall at $z = L$ is considered rigid, so that $\partial P/\partial z = 0$:

$$B_G = A_G e^{i2q_G L}. \tag{S18}$$

Then, both pressure field and velocity field can be written as

$$P(\boldsymbol{r}) = \sum_{\boldsymbol{G}} A_G \cos\left(q_G(z-L)\right) e^{iq_G L} e^{i\boldsymbol{k_G}\cdot\boldsymbol{r}} \tag{S19}$$

and the normal velocity

$$v_n(\boldsymbol{r}) = \sum_{\boldsymbol{G}} \frac{-q_G}{k_b Z_b} 2A_G \sin\left(q_G(z-L)\right) e^{iq_G L} e^{i\boldsymbol{k_G}\cdot\boldsymbol{r}}. \tag{S20}$$

Field inside the holes is equal to the one use for the previous case (equations S4 and S5), and the same mode matching technique is applied, obtaining

$$\sum_{\boldsymbol{G}} 2A_G \cos\left(q_G L\right) e^{iq_G L} e^{i\boldsymbol{G}\mathbf{R}_\alpha} H_{\alpha G} = B_\alpha \cot\left(k_b L_\alpha\right) \tag{S21}$$

and

$$\frac{2q_G}{k_b} A_G \sin\left(q_G L\right) e^{iq_G L} = -\sum_\beta B_\beta f_\beta e^{-i\boldsymbol{G}\mathbf{R}_\beta} H_{\beta G}, \tag{S22}$$

which, combined,

$$\sum_{\beta=1}^{N} [\delta_{\alpha\beta} \cot\left(k_b L_\alpha\right) + \chi_{\alpha\beta}] B_\beta = 0, \tag{S23}$$

where $\chi_{\alpha\beta}$ is, after simplification of $H_{\alpha G}$,

$$\chi_{\alpha\beta} = \sum_{\boldsymbol{G}} \frac{k_b}{q_G} \cot\left(q_G L\right) f_\beta e^{i\boldsymbol{G}\mathbf{R}_{\alpha\beta}} \frac{4}{R_a^2 |\boldsymbol{k_G}|^2} J_1^2(R_a|\boldsymbol{k_G}|). \tag{S24}$$

Repeating the same steps as for the uncovered case, the summation over $\mathbf{G}$ is transformed into an integral over $\mathbf{k}$, and further change of coordinate system and the application of the addition theorem gives the following expression for $\chi_{\alpha\beta}$.

$$\chi_{\alpha\beta} = 2\sum_{n=-\infty}^{+\infty}(-1)^n e^{2\pi n i\alpha/N} e^{-2\pi n i\beta/N} I_{cov}(n), \tag{S25}$$

where

$$I_{cov}(n) = \int_0^{+\infty} \frac{k_b}{q_k k}\cot(q_k L) J_n^2(kR_0) J_1^2(kR_a) dk. \tag{S26}$$

In this occasion, $I_{cov}(n)$ is always real, as $\cot(ix) = -i\coth(x)$. Thus, after applying condition (S15) to the system in equation (S23), only one condition is obtained for the design of bound states in the continuum

$$-\frac{1}{2}\cot(k_b L_\alpha) = \sum_{n=-\infty}^{\infty}(-1)^n I_{cov}(n)\sum_{\beta=1}^{N} e^{2\pi i\beta(\ell-n)/N}, \tag{S27}$$

where summation term $\sum_{\beta=1}^{N} e^{2\pi i\beta(\ell-n)/N}$ is equal to N if and only if $n=\ell$, and 0 otherwise. Finally,

$$-\cot(k_b L_\alpha) = 2N(-1)^\ell I_{cov}(\ell). \tag{S28}$$

As $\cot(x)$'s domain is $\mathbb{R}$ and the result of the integral term is a real number, a solution for the equation can always be found, proving that a bound state in the continuum can be designed in the covered case.

The equations have been numerically implemented, and real values have been obtained for the geometrical parameters of the structure and the operating frequency of the BIC. The resulting eigenmode is depicted in Fig. 1 panel b in the main document. The geometrical features of the structure are: $L = 2.5$ cm, $L_\alpha = 1.36$ cm, $R_0 = 5.61$ cm and $R_a = 5.9$ mm. The frequency at which the mode is designed is 5 kHz, but it is obtained in simulations with a small shift at 5010.9 Hz. Regarding the vertical planes, Supplementary Figure 1 shows the vertical planes of the waveguide at different angles, where each plane is showing two of the resonators of the structure.

SUPPLEMENTARY NOTE 3: RESONANT IMPEDANCE MODEL FOR DRILLED HOLES IN A WAVEGUIDE

Let us consider the geometry shown if Supplementary Figure 2, where we assume that propagation in the waveguide is mainly dominated by the fundamental mode, which has a constant pressure level along the z direction. However, inside the hole, the waveguide has a higher height, so that more modes are allowed then. Thus, for the multipolar symmetry q, we will have that the continuity of the pressure field at $r = a$,

$$A_q J_q(k_b a) + B_q H_q(k_b a) = \sum_{n=0}^{\infty} C_q^n J_q(k_n a)\cos\frac{n\pi}{L}z \tag{S29}$$

while that of the particle velocity will be

$$A_q J_q'(k_b a) + B_q H_q'(k_b a) = \sum_{n=0}^{\infty} \frac{k_b}{k_n} C_q^n J_q'(k_n a)\cos\frac{n\pi}{L}z \tag{S30}$$

Applying mode matching theory we find the following system of equations

$$A_q J_q(k_b a) + B_q H_q(k_b a) = \sum_{n=0}^{\infty} C_q^n J_q(k_n a)\,\mathrm{sinc}\,(\frac{n\pi}{L+L_\alpha}L) \tag{S31}$$

$$\left(A_q J_q'(k_b a) + B_q H_q'(k_b a)\right) L\,\mathrm{sinc}\,(\frac{n\pi}{L+L_\alpha}L) = \frac{k_b}{k_n} C_q^n J_q'(k_n a)\frac{1}{2}(L+L_\alpha) \tag{S32}$$

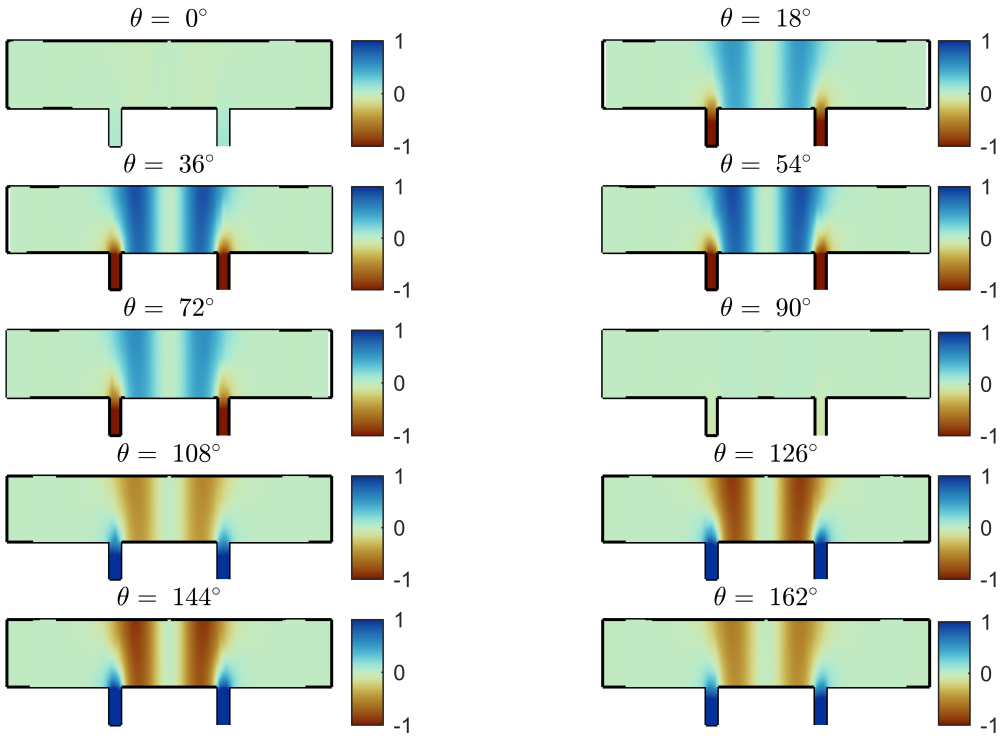

Supplementary Figure 1: Vertical section of the BIC mode at different angles.

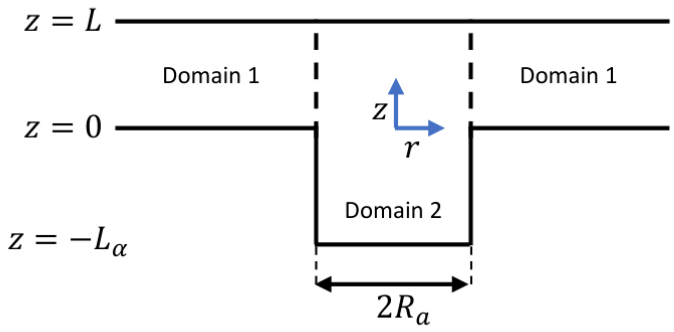

Supplementary Figure 2: Illustration of the geometry for the impedance computation.

which can be cast as

$$A_q J_q(k_b a) + B_q H_q(k_b a) = Z_q \left(A_q J_q'(k_b a) + B_q H_q'(k_b a) \right) \tag{S33}$$

where

$$Z_q = \sum_{n=0}^{\infty} \frac{k_n}{k_b} \frac{J_q(k_n a)}{J_q'(k_n a)} \frac{2L}{L + L_\alpha} \operatorname{sinc}^2\left(\frac{n\pi}{L + L_\alpha} L\right) \tag{S34}$$

as we see, the response of the hole is that of a resonant impedance. Following [4], for long wavelengths relative to

the radius of the hole only the terms $q = 0, \pm 1$ are relevant, and the ones who define the effective behaviour of the inclusion. Supplementary Figure 3 shows Z_q for $q = 0, 1$, showing the resonant behaviour within the frequency range of interest.

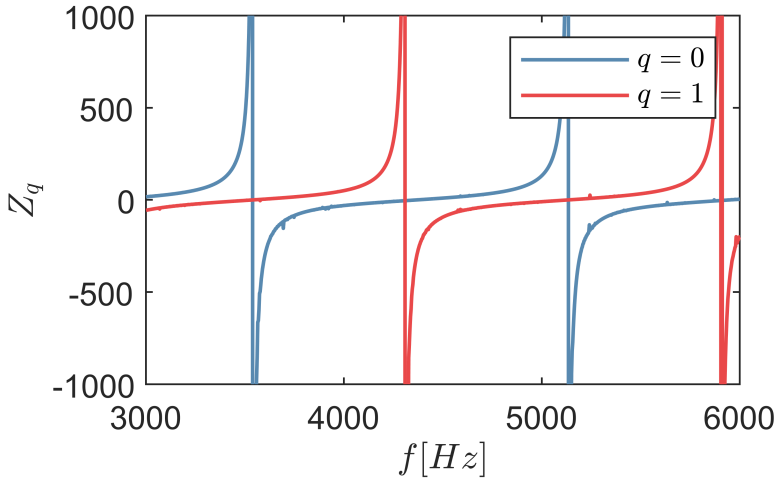

Supplementary Figure 3: Impedance evolution for $q = 0$ and $q = 1$ given the following geometrical configuration; $R_0 = 5.61$ cm, $L = 2.5$ cm, $L_\alpha = 1.36$ cm and $R_a = 6$ mm.

SUPPLEMENTARY NOTE 4: EXPERIMENTAL SETUP

Supplementary Figure 4 shows a picture of the experimental setup, being Fig. 1 panel **a** in the main document a schematic section of it. In the picture, the acoustic waveguide is completely seen thanks to the transparent top glass cover.

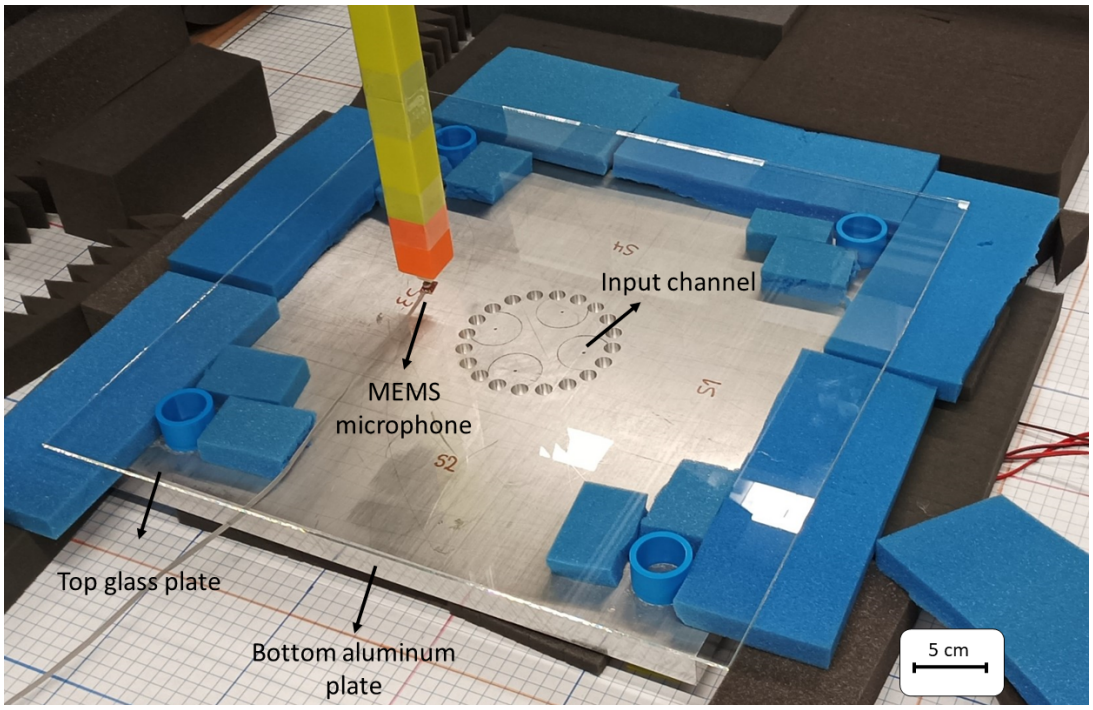

Supplementary Figure 4: Photography of the experimental setup.

The MEMs microphone is introduced inside the waveguide and attached to the top cover by means of a magnet. On the other side of the top cover (i.e., the exterior of the system), another magnet glued to a XYZ scanning system drives the movement of the microphone. The glass cover is thin enough to allow both magnets to interact. Moreover, the scanning is performed such that the possible mismatch of position between the scan and the microphone gets compensated. The excitation system cannot be seen in the photo. Nevertheless, the four throughout holes can be seen inside the circular cluster, and the position of the loudspeakers is right on the bottom of the alumina plate facing the passing holes. The foam is surrounding the structure in order to avoid reflections coming from the change of acoustic impedance at the edges of the waveguide, even if we assume that most of the energy will remain confined in the inner part of the cluster.

The excitation signal was a Gaussian pulse that covered a frequency range around 5 kHz. Therefore, not only the BIC could be excited, but other resonances with the same symmetry as the excitation system can be excited. This is the case for the one shown in Supplementary Figure 5. This resonance is found in the eigenmode analysis of Comsol with a quality factor of 4.12. In the experimental results, the resonance is hidden by the BIC, however if we analyse the spectra excited, we will be able to find the same scattering field as was expected by the eigenmodes. By taking a look at the line $y = 0$, we can realize that there is a good agreement between simulation and experiment.

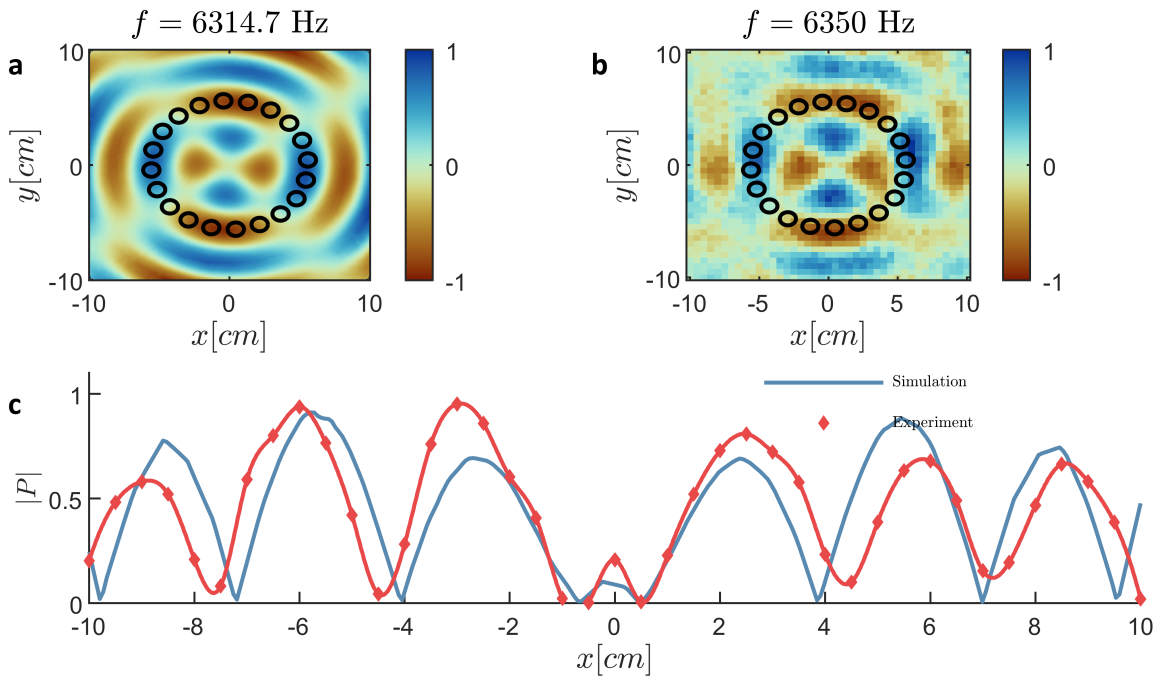

Supplementary Figure 5: Resonant mode measured in the structure. Panels **b** and **c** show the BIC normalized real pressure field both in simulation (**b**) and in experiment (**c**). Panel **d** depicts the normalized absolute pressure field for the line $y = 0$.

SUPPLEMENTARY NOTE 5: EXPERIMENTAL MEASUREMENTS UNCOVERED PLATE

Experimental measurements with the uncovered plate have been performed. The results are summarized in figures 6 and 7. Supplementary Figure 6 panel **a** shows an illustration of the geometry of the plate. The geometrical parameters have been stated in the main text: $R_0 = 5.6cm$, $R_\alpha = 5.9mm$ and $L_\alpha = 1.35cm$. Panels **b** and **c** show the energy distribution of the $\ell = 2$ mode both for experiment and simulation respectively. Red dot in panel **b** indicates the spatial position at which temporal measurements have been performed and later shown in Supplementary Figure 7. The mode shape has been normalized in both cases with respect to the maximum value found for the mode. Finally, panel **d** depicts the normalized absolute pressure field for the line with $y = 0$. Even if there is a good agreement between experiment and simulation, the result is not as good as the one shown in the main article for the covered case.

Supplementary Figure 7 shows the analysis of the uncovered plate for a temporal measurement performed at the red point in Supplementary Figure 6 panel **b**. Panel **a** gives the temporal signal and its envelope, both for the scattered (blue) and the incident field (red). Compared to the same figure shown for the covered case in the main article, the tail of the scattered field is much shorter, indicating that there is no high-quality resonance present in the structure. Furthermore, the scattered signal gets completely masked by the incident signal, while in the main article one can see a field enhancement for the scattered field. Panel **b** shows the spectral content of both the incident and the scattered field. Both fields have been normalized for the sake of having a better visualization. It can be seen that the scattered field has its peak at the mode frequency. Even though, compared to the spectral response with the covered plate, the resonance is really wide. Panel **c** shows the ratio between the scattered spectrum and the incident one. The peak for this ratio is found at the mode frequency $\sim 5015Hz$. Once again, this result differs from the one found in the main article for the covered case: there is no ratio higher than one, indicating that there is no field enhancement at any frequency, while the covered plate showed a huge enhancement near the mode frequency.

SUPPLEMENTARY REFERENCES

* dtorrent@uji.es

[1] D. Torrent, Acoustic anomalous reflectors based on diffraction grating engineering, Physical Review B **98**, 060101 (2018).

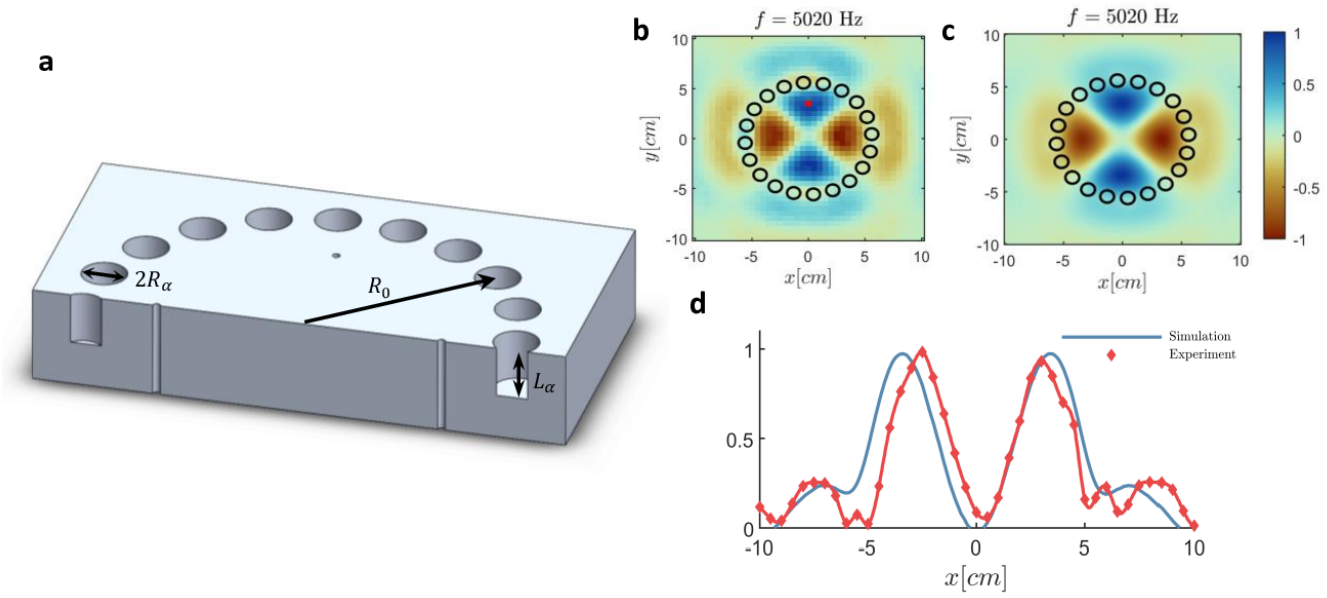

Supplementary Figure 6: Designed plate and performance. Panel **a** shows an illustration of a section of the plate, with the input channels used for the external excitation. Panels **b** and **c** show the real pressure field of the mode both in experiment (**b**) and in simulation (**c**). Panel **d** depicts the normalized absolute pressure field for the line $y = 0$, showing good agreement between simulation and experiment.

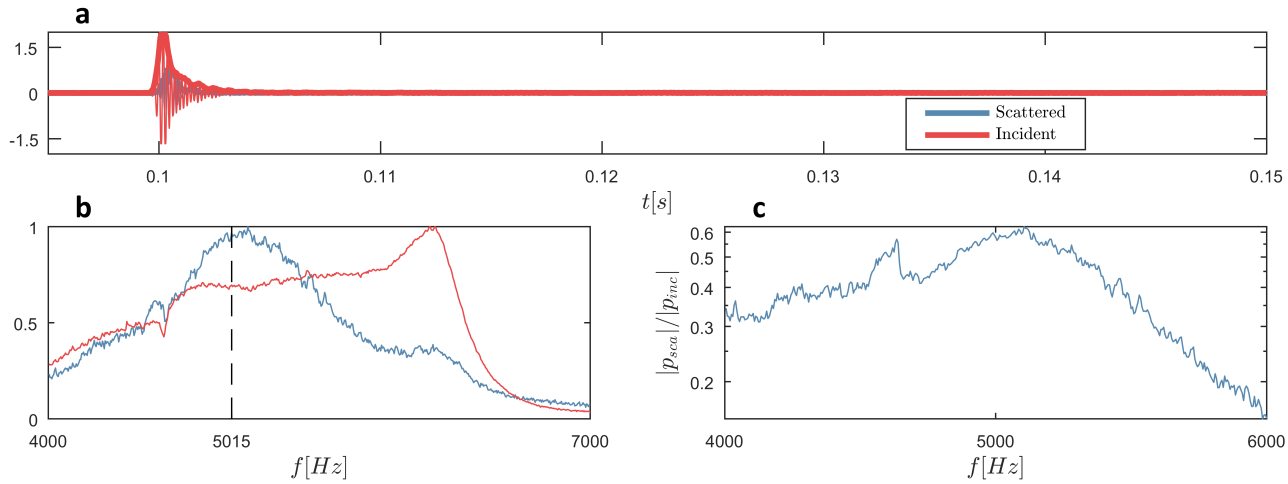

Supplementary Figure 7: Experimental results from the uncovered $\ell = 2$ designed plate. Panel **a** shows the incident and scattered signal and envelope at a given position ($x = 0$, $y = 35mm$, $z = 22mm$). Panel **b** shows the normalized spectrum for both the incident and the scattered field. Panel **c** shows the ratio between the scattered spectrum and the incident one in the experiment.

[2] M. Martí-Sabaté, B. Djafari-Rouhani, and D. Torrent, Bound states in the continuum in circular clusters of scatterers, Phys. Rev. Res. **5**, 013131 (2023).

[3] H. Putley, G. Chaplain, H. Rakotoarimanga-Andrianjaka, B. Maling, and R. Craster, Whispering-bloch elastic circuits, Wave Motion **105**, 102755 (2021).

[4] D. Torrent and J. Sánchez-Dehesa, Multiple scattering formulation of two-dimensional acoustic and electromagnetic metamaterials, New Journal of Physics **13**, 093018 (2011).